ChemPubSoc Europe
DOI: 10.1002/ejic.201900807
EurJIC European Journal of Inorganic Chemistry
Full Paper

Oxovanadium Catalysts

Selective C_α Alcohol Oxidation of Lignin Substrates Featuring a β-O-4 Linkage by a Dinuclear Oxovanadium Catalyst via Two-Electron Redox Processes

Yan-Ting Tsai,[a] Chih-Yao Chen,[a] Yi-Ju Hsieh,[a] and Ming-Li Tsai*[a]

Abstract: Developing highly efficient catalyst systems to transform lignin biomass into value-added chemical feedstocks is imperative for utilizing lignin as renewable alternatives to fossil fuels. Recently, the pre-activated strategy involving the selective oxidation of C_α alcohol of lignin substrates containing (β-O-4 linkage mode has been demonstrated to significantly increase the depolymerization efficiency of native aspen lignin from 10–20 to 60 wt.-%. In this study, we reported the synthesis of a dinuclear oxovanadium complex **2** that is capable of selectively oxidizing the C_α alcohol (80 – 100% selectivity) of various dimeric lignin substrates under a mild condition. Further investigation of catalytic mechanism has revealed that two V=O motifs of complex **2** could serve as proton abstraction sites for both C_α and C_γ alcohol of dimeric lignin substrates, respectively. Interestingly, the dinuclear vanadium intermediate **4** demonstrates the ability to uptake two electrons resulting from the oxidation of C_α alcohol and yields two corresponding mononuclear V^{IV} intermediate **5**. The mononuclear V^{IV} intermediate **5** exhibits a characteristic 8-line EPR spectrum and possesses one unpaired electron determined by the Evans method. The established structure-reactivity relationships will be able to shed light on the future directions for rational design of highly efficient catalysts for selective oxidation of lignin biomass.

Introduction

The over-exploitation of limited natural resources resulting from exponential growth of human population is destined to the depletion of fossil fuels and projected shortages of commodity chemicals in the near future. To achieve sustainable energy society, the development of technologies to harness renewable resources as alternatives to fossil fuels is imperative. Lignocellulose biomass from agricultural residues and wood wastes produced annually is promising non-edible sources due to their diverse chemical compositions consisted of versatile aliphatic and aromatic building blocks.[1] In particular, lignin biomass, the natural polymer consisting of methoxy-substituted phenolic monomers, is the only abundant source of renewable aromatics from biomass.[2] Despite there are existing processes (gasification, pyrolysis, liquid phase reforming, acid/base catalyzed depolymerization) for converting lignin biomass into value-added chemical feedstocks, harsh conditions (high temperatures/pressures or using strong acid/base) have limited their energy efficiency and environmental sustainability.[3]

The chemical structures of lignin biomass are comprised of the polyphenolic compounds with versatile linkage modes including β-O-4 (β-aryl ether), β-5 (phenylcoumaran), β-β (resinol), and β-1 (spirodienone), etc.[4] Despite the diverse patterns of linkage modes distributed in different agricultural residues and wood wastes, the β-O-4 linkage mode is the most abundant component which accounts for 40 – 65% of total linkages presented in lignin biomass. Recently, the C–O/C–C bond cleavage of lignin model substrates or depolymerizations of natural lignin have been demonstrated via redox-neutral,[5] acid/base,[6] and oxidative[3d,5g,6e,7] catalyst systems. In particular, the selectivity toward C–O and C–C bond cleavage of lignin model substrates containing the β-O-4 linkage mode have been successfully catalyzed by a five-coordinate vanadium-salen complex and a six-coordinate $(HQ)_2V(O)(O^iPr)$ mononuclear oxovanadium catalysts, respectively.[7a,7d,8] The facile non-oxidative C–O bond cleavage catalyzed by the five-coordinate oxovanadium complex has been proposed via a ketyl radical intermediate generating from a one-electron process[7b] and also been shown to depolymerize lignin samples isolated from *Miscanthus giganteus* pretreated with organosolv processes.[9]

In addition to the photocatalytic carbon–carbon bond cleavage reaction facilitated by vanadium catalysts,[10] the two-step strategy regarding the selective oxidation of C_α alcohol into ketone followed by formic acid-induced C–O bond cleavage has been developed. The approach has significantly improved the depolymerization efficiency of native aspen lignin samples from less than 10–20 wt.-% yields up to more than 60 wt.-%.[11] The dramatic increase of depolymerization yield is attributed to the weakening of C_β-O bond strength by 15 kcal/mol resulting from the selective oxidation of C_α alcohol to ketone as shown in Scheme 1.[11,12] Although the catalytic oxidation of C_α alcohol of lignin substrates containing β-O-4 linkage modes have been presented by either microwave-assisted photocatalysis,[13] tran-

---

[a] *Department of Chemistry, National Sun Yat-sen University, Kaohsiung 80424, Taiwan*
E-mail: mltsai@mail.nsysu.edu.tw
http://chem.nsysu.edu.tw/var/file/180/1180/img/780/ml_tsai_c.htm
Supporting information and ORCID(s) from the author(s) for this article are available on the WWW under https://doi.org/10.1002/ejic.201900807.

sition metal catalysts[3d,7m] or AcNH-TEMPO/HNO_3/HCl catalyst system,[12c] the development of a highly efficient catalyst system that uses less-expensive additives under relatively mild reaction conditions (weak acids/bases or O_2 in air) will be necessary for large-scale industrial applications.

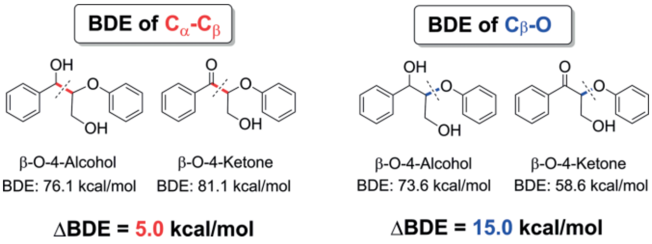

Scheme 1. Differences in bond dissociation energies of C_α-C_β and C_β-O linkage modes between β-O-4-alcohol and β-O-4-ketone lignin model substrates.

Here, we presented the synthesis of dinuclear oxovanadium catalysts with tridentate [O,N,O] ligation mode.[14] The dinuclear oxovanadium catalyst was characterized by single-crystal X-ray diffraction, IR, ^{51}

V-NMR, and cyclic voltammetry. The dinuclear vanadium catalyst **2** has shown excellent selectivity of oxidizing the C_α alcohol of dimeric lignin substrates containing β-O-4 linkage mode into ketone. The unique selectivity of catalytic alcohol oxidation has been attributed to the nature of dinuclear vanadium core that is capable of acting as a two-electron reservoir evidenced by its cyclic voltammogram exhibiting one reversible and one quasi-reversible redox couples. The detailed catalytic mechanism has further been delineated via a combination of ^{1}H-NMR, 2D-NMR (COSY, HSQC), electron paramagnetic resonance (EPR) spectroscopy and Evans method.

Results and Discussion

Synthesis and Characterization of Mononuclear and Dinuclear Oxovanadium Complexes

The mononuclear oxovanadium complex **1** chelated with tridentate [O,N,O] salicylaldehyde benzoyl hydrazone (SBH–H_2) ligand was successfully synthesized by dropwise addition of $V(O)(O^iPr)_3$ into the MeOH solution of SBH-H_2 tridentate ligand at room temperature as reported in literature.[10b] The reaction was monitored by the disappearance of characteristic IR $\nu_{C=O}$ stretching frequency of SBH-H_2 at 1676 cm^{-1} and the red shift of $\nu_{C=N}$ (free ligand: 1606 cm^{-1}; chelated ligand 1601 cm^{-1}), respectively. The resulting mononuclear oxovanadium complex $[VO(OCH_3)(CH_3OH)SBH]$ (**1**) is best described as distorted octahedral geometry. SBH-H_2 is deprotonated by two coordinated O^iPr ligands of $V(O)(O^iPr)_3$ and provides tridentate [O,N,O] ligation to the complex **1**. The coordinated methoxide ligand of complex **1** is resulting from a simple ligand-exchange reaction between the third coordinated O^iPr ligand of $V(O)(O^iPr)_3$ and MeOH solvent (Scheme 2).

By adding one equivalent of H_2O into the THF solution of complex **1** at room temperature, the corresponding dinuclear oxovanadium complex [(SBH)(O)V(μ-O)V(O)(SBH)] (**2**) was produced in nearly quantitative fashion (96% yield). The reaction is presumably proceeded by protonating the coordinated methoxide ligands from two complex **1** via H_2O to produce two CH_3OH molecules and O^{2-} serving as a bridged ligand for two resulting V(O)(SBH) fragments. To quantitatively understand the redox behavior of the synthesized oxovanadium complexes, the cyclic voltammetry of complexes **1** and **2** were conducted in CH_3CN solution with 0.1 M $[^nBu_4N][PF_6]$ acting as supporting electrolyte at room temperature. Complex **1** shows one reversible redox process at $E_{1/2}$ = –0.477 V (vs. Fe^+/Fe), which is attributed to a reversible $V^{V/IV}$ redox couple, with ΔEp = 86 mV and i_{pa}/i_{pc} = 0.70 (red line, Figure 1). On the contrary, complex **2** displays one reversible redox couple at $E_{1/2}$ = 0.055 V (vs. Fe^+/Fe) with ΔEp = 83 mV, i_{pc}/i_{pa} = 0.74 and one irreversible reduction wave at E = –0.335 V (vs. Fe^+/Fe) (green line, Figure 1). The two redox couples of complex **2** were tentative assigned as V^V-V^V/V^V-V^{IV} and V^V-V^{IV}/V^{IV}-V^{IV}, respectively. The significant positive $E_{1/2}$ of complex **2** as compared to that of complex **1** (–0.477 V for **1** and 0.055 V for **2**) indicates that the complex **2** is much easier to accept one electron than complex **1**. In addition, the irreversible behavior of the second reduction wave of complex **2** implicates its ability to accept an additional electron to form an electrochemically unstable V^{IV}-V^{IV} intermediate. The diamagnetic nature of complexes **1** and **2** are demonstrated by their ^{1}H and ^{13}C NMR spectra that display similar chemical shift and splitting pattern as compared to free SBH-H_2 ligand (Figure S1–S6). In addition, the ^{51}V NMR of complexes **1** and **2** were determined as δ = –548 ppm and δ = –577 ppm, respectively, which could serve as spectroscopic references to monitor the possible structural change of oxovanadium complexes during chemical transformations/catalytic reactions (Figure S7 and S8). Note that the two redox waves of complex **2** both exhibit

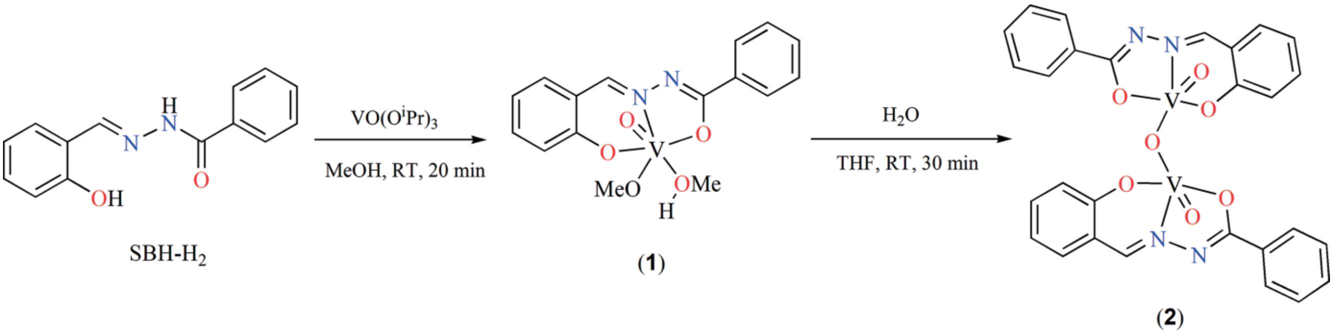

Scheme 2. Synthetic procedures of complex **1** and **2**.

anodic shifts relative to the redox wave corresponds to the V^V/V^{IV} of complex **1** could be attributed to the electrophilic nature of 5 C.N. vanadium center in complex **2** as compared to the 6 C.N. coordination environment in complex **1.** Nevertheless, the detailed studies of coupling interactions between two vanadium centers of complex **2** with different redox states (V^V-V^V/V^V-V^{IV} and V^V-V^{IV}/V^{IV}-V^{IV}) will be required in order to provide more insights on this observation.

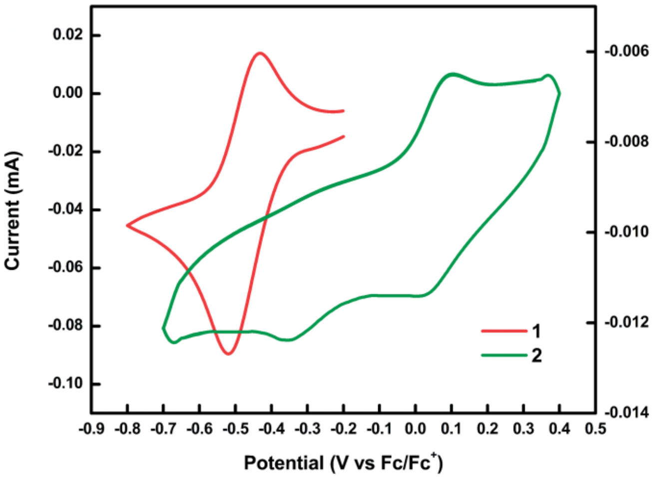

Figure 1. The cyclic voltammograms of complexes 1 (red) and 2 (green) in 0.1 M [^{n}Bu$_4$N][PF$_6$] supporting electrolyte with a glass carbon working electrode at a scan rate of 50 mV.

The ORTEP plot and the selected bond lengths and bond angles of complex **2** are shown in Figure 2. The dimeric structure of complex **2** consists of two five-coordinate monomeric vanadium units bridged by an O^{2-} ligand. The local geometry of vanadium center could be determined by structural parameter τ_5 ($\tau_5 = (\beta-\alpha)/60^o$ where α and β are the two greatest valence angles of the coordination center and $\beta > \alpha$). The τ_5 of vanadium center is calculated as ca. 0.02 (α: ∡O(1)–V(1)–O(2) ca. 148°; β: ∡N(1)–V(1)–O(3) ca. 149°). Therefore, the local vanadium geometry of complex **2** is best described as square pyramidal (square pyramidal: τ_5 = 0; trigonal bipyramidal: τ_5 = 1) where the V=O fragment located at an apical position. The alterations of coordination numbers (C.N. = 6 and C.N. = 5 for complexes **1** and **2,** respectively) and coordination environments (O_5N_1 and O_4N_1 donor sets for complexes **1** and **2**, respectively) between complexes **1** and **2** also manifest in the differences in their metal-ligand bond lengths. The bond length of V=O bond in complex **2** is slightly shorter than that of complex **1** (V(1)–O(3) 1.5890(16) for complex **1**; V(1)–O(4) 1.5756(14) for complex **2**) and average V–O bond length provided by the SBH^{2-} ligand in complex **2** is also ca. 0.018 Å shorter than that in complex **1**. The decrease of V=O and average $V–O_{SBH}$ bond lengths from complex **1** to complex **2** suggest that the relatively electron deficient nature of vanadium center in complex **2** which is consistent with the cyclic voltammetry studies associated V^V/V^{IV} and $V^VV^V/V^{IV}V^V$ redox couples ($E_{1/2}$ = −0.477 for complex **1** and $E_{1/2}$ = 0.055 for complex **2**) of complexes **1** and **2**, respectively.

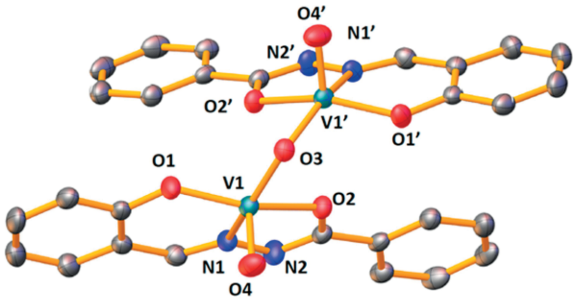

Figure 2. ORTEP drawing and labeling scheme of 2 with thermal ellipsoid drawn at 50% probability and selected bond lengths [Å] and angles [deg]. Hydrogen atoms are omitted for clarity. Complex 2: V(1)–N(1) 2.0893(17), V(1)–O(1) 1.8205(11), V(1)–O(2) 1.9541(12), V(1)–O(3) 1.8029(10), V(1)–O(4) 1.5756(14), V(1)–V(1′) 2.9948(6), O(3)–V(1)–O(4) 107.32(7), O(1)–V(1)–O(4) 103.33(7), O(1)–V(1)–O(3) 104.78(5), O(2)–V(1)–O(4) 102.74(7), O(2)–V(1)–O(3) 84.82(5), O(1)–V(1)–O(2) 147.91(6), N(1)–V(1)–O(4) 99.18(8), N(1)–V(1)–O(3) 149.24(7), N(1)–V(1)–O(1) 83.47(6), N(1)–V(1)–O(2) 74.18(6), V(1)–O(3)–V(1′) 112.31(9).

Synthesis of Dimeric Lignin Model Substrates Containing β-O-4 Linkage Modes

To explore the chemical reactivity of oxovanadium complexes **1** and **2**, a series of dimeric lignin substrates containing β-O-4 ether bond were synthesized. The β-O-4 linkage was incorporated by the reaction of 2-bromo-1-phenylethanone or its *para*-methoxy derivatives with phenoxide or its *ortho*-methoxy derivative, respectively. This synthetic route will allow us to synthe-

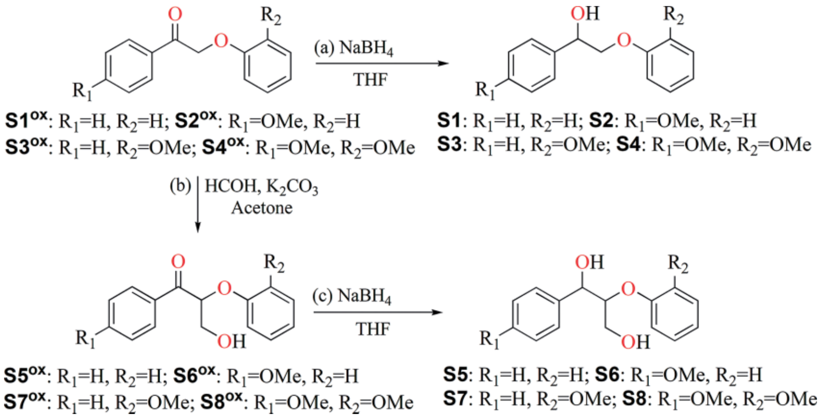

Scheme 3. Synthetic procedures of lignin model substrates (S1–S8 and S1^{ox}–S8^{ox}) containing a β-O-4 linkage mode.

size dimeric lignin substrates **S1**^{ox}–**S4**^{ox} which could serve as starting materials to yield the corresponding alcohol substrates **S1**–**S4** via the nucleophilic attack of $NaBH_4$ at the C_α position (Scheme 3a). The oxidized dimeric lignin substrates with aliphatic alcohol functional group at the C_α position **S5**^{ox}–**S8**^{ox} could be obtained by the addition of HCOH into **S1**^{ox}–**S4**^{ox} in the presence of K_2CO_3 (Scheme 3b). The addition of $NaBH_4$ into a THF solution of **S5**^{ox}–**S8**^{ox} results in the formation of the corresponding **S5**–**S8** (Scheme 3c) which closely resembles to the chemical structure of natural lignin substrates featuring a secondary benzylic alcohol and a primary aliphatic alcohol at the C_α and C_γ positions, respectively. Note that the tested substrates do not cover the common set of dimeric lignin model substrates such as disubstituted guaiacyl analog and trisubstituted syringyl analog. From the systematic studies of catalytic reactivity of the oxovanadium complexes **1** and **2** toward the synthesized dimeric lignin substrates **S1**–**S8**, the electronic effects of the methoxy substituent on the aromatic ring and the incorporation of primary aliphatic alcohol at the C_γ positions could be elucidated.

Selective Alcohol Oxidation Catalyzed by Oxovanadium Complexes

To investigate the catalytic oxidation of secondary benzylic alcohol of dimeric lignin substrates by oxovanadium complexes **1** and **2**, the simplest synthesized lignin substrate containing β-O-4 linkage **S1** was chosen to screen an optimized catalytic condition. As shown in Table 1, **S1** was treated with the 10 mol % of complex **1** and 5 mol % of complex **2**, respectively, at 80 °C under air for 24 hours in different solvents. In CH_3CN or toluene solvent, both complexes **1** and **2** show very low conversions (< 10%) of oxidizing the C_α alcohol of **S1** into the C_α ketone of **S1**^{ox} (entries 1, 2, 6, 7). The efficiency of catalytic oxidation of **S1** into **S1**^{ox} in DMF solvent slightly increases to 36.2% and 39.0% for complexes **1** and **2** (entries 3, 4, 8, 9), respectively. Interestingly, using pyridine as a solvent achieves almost 100% conversion of **S1** (95% for both complex **1** and **2**). Unlike complex **2** remains intact during the catalytic reactions, the transformation of complex **1** into complex **2** has been observed and characterized by ^{51}V-NMR spectroscopy (Figure S9). Taking advantage of the robustness of complex **2**, the catalytically oxidizing the C_α alcohol of the synthesized dimeric lignin substrates into ketone will be further pursued by the complex **2**.

Table 1. Solvent effects on the catalytic oxidation of S1 into S1^{ox}.

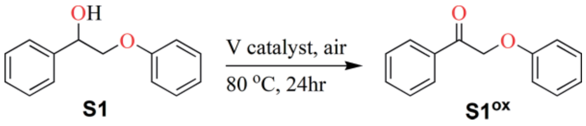

Entry	Catalyst[mol %]	Solvent	Conversion%	Yield[a]%
1	10% **1**	CH_3CN	4.9	2.7
2	10% **1**	Toluene	2.8	1.0
3	10% **1**	DMSO	23.4	13.4
4	10% **1**	DMF	36.2	29.0
5	10% **1**	pyridine	95.0	45.2
6	5% **2**	CH_3CN	8.0	2.7
7	5% **2**	Toluene	6.2	4.0
8	5% **2**	DMSO	5.0	5.0
9	5% **2**	DMF	39.0	20.0
10	5% **2**	pyridine	97.0	47.5

[a] Conversions and yields determined by integration against an internal standard 2-(trimethylsilyl)ethanol.

The effects of pyridine on the transformation of **S1** into **S1**^{ox} were studied by using pyridine as an additive in the catalytic system containing 5 mol % of complex **2** at 80 °C under air for 24 hours in CH_3CN solution. As shown in Table 2, the conversion of **S1** is significantly enhanced from 5.4% to 100% as additive pyridine increase from 10 mol % to 1 equivalent (Table 2, entries 1–3), respectively. Increasing the amount of pyridine added to 2 or 4 equivalents only slightly lowers the selectivity of catalytic oxidation of the C_α alcohol from 100% to 80% (Table 2, entries 4 and 5). Therefore, 1 equivalent of pyridine is the optimal amount in order to achieve both excellent selectivity and efficiency of converting **S1** into **S1**^{ox}. To exclude the possibility of pyridine serving as a catalyst, the catalytic condition of one equivalent pyridine in CH_3CN solvent at 80 °C under air for 24 hours was conducted. As shown in the entry 6 of Table 2, 0% of conversion has been observed.

Table 2. Additive effects on the oxidation of S1 into S1^{ox}.

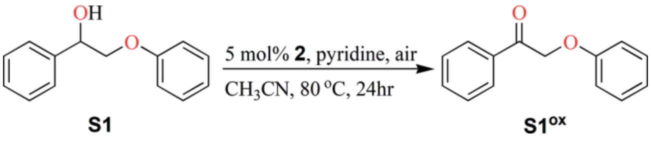

Entry	Cat.[mol %]	Loading	Additive[a]	Conv.%	Yield[b]%
1	**2**	5%	10 mol %	5.4	3,5
2	**2**	5%	20 mol %	20.2	15.4
3	**2**	5%	1 eq	100.0	100.0
4	**2**	5%	2 eq	100.0	79.7
5	**2**	5%	4 eq	100.0	80.0
6	–	–	1 eq	0	0

[a] The amount of pyridine. [b] Conversions and yields determined by integration against an internal standard 2-(trimethylsilyl)ethanol.

The substrate scope has been examined with the synthesized substrates **S1–S8** under the established reaction condition (5 mol % loading of catalyst **2** with 1 equivalent pyridine as additive in CH_3CN solution at 80 °C under air for 24 hours). The incorporation of methoxide functional group either on R^1 or R^2 positions has slightly lowered conversion from 100% for **S1** to ca. 90% for **S2** and **S3**, respectively, over the course of 24 hours (Table 3, entries 2 and 3). If both R^1 and R^2 positions are substituted with methoxy group, the conversion from **S4** to **S4**^{ox} has decreased to 70% (Table 3, entry 4) which indicates the incorporation of electron-donating groups on the aryl ring of lignin substrates containing β-O-4 linkage has notably lowered conversion efficiency in the current catalyst system.

To further explore the reactivity and selectivity of complex **2** toward the substrates that closely resemble to natural lignin, the catalytic oxidation of C_α alcohol of substrates containing primary aliphatic CH_2OH moiety on the C_β position (**S5**–**S8**) was investigated. The catalytic conversion efficiency of C_α alcohol into the corresponding ketone for **S5**–**S8** is 10–30% lower

Table 3. Substrate scope of selective oxidation of dimeric lignin substrates.

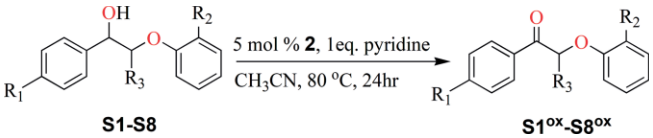

Entry	Substrate/Product	R^1	R^2	R$_3$	Con.%	Yield[a]%	Sel.%
1	**S1/ S1^{ox}**	H	H	H	100	100	100
2	**S2/S2 ^{ox}**	OMe	H	H	93	87	94
3	**S3/S3 ^{ox}**	H	OMe	H	90	70	78
4	**S4/S4 ^{ox}**	OMe	OMe	H	70	66	94
5	**S5/S5^{ox}**	H	H	CH_2OH	77	75	97
6	**S6/S6 ^{ox}**	OMe	H	CH_2OH	65	58	89
7	**S7/S7 ^{ox}**	H	OMe	CH_2OH	62	53	85
8	**S8/S8 ^{ox}**	OMe	OMe	CH_2OH	61	53	87

[a] Conversions and yields determined by integration against an internal standard 2-(trimethylsilyl)ethanol.

(Table 3, entries 5–8) than that for substrates **S1**–**S4**. In addition, the effects of different bases (including pyridine, K_2CO_3, $NaHCO_3$, DBU, $CsCO_3$, Et_3N) on the selective oxidation of S_5 to $S5^{ox}$ have been examined; only pyridine demonstrates a significant conversion (77%) and selectivity (97%). All the other bases show less than 16% of conversion (Table S1 and Figure S10). Notably, the oxidation of primary aliphatic C_γ alcohol to aldehyde has not been observed in the current catalyst system which indicates the complex **2** could selectively oxidize electron-deficient secondary benzylic alcohol over electron-rich primary aliphatic alcohol with 85 – 96% selectivity.

Mechanistic Studies of Catalytic Alcohol Oxidation of Dimeric Lignin Substrates via Dinuclear Oxovanadium Complex 2

In order to elucidate the mechanism associated with the highly selective oxidation of C_α alcohol to the corresponding ketone catalyzed by dinuclear oxovanadium complex **2**, the transformation of **S5** into **S5^{ox}** via complex **2** was delineated step-by-step consisting of (a) the coordination of 2 equivalent pyridine to the vacant site of vanadium center of complex **2** (b) the proposed structure of oxovanadium-substrate complex **4** resulting from the stoichiometric reaction among complex **2**, pyridine and **S5**; (c) exploring the role of additive by reacting the oxovanadium-substrate complex **4** with pyridine; (d) the spectroscopic characterizations of a key dinuclear oxovanadium intermediate **5** produced by uptaking two electrons from the oxidation of C_α alcohol to ketone; (e) regenerating dinuclear oxovanadium complex **2** by reacting intermediate **5** with O_2 to complete the catalytic cycle. The proposed elementary steps of the catalytic cycle were studied by the utilizations of ^{1}H NMR, ^{51}V NMR, 2D-NMR including Correlation Spectroscopy (COSY), Heteronuclear Single-Quantum Correlation (HSQC), Heteronuclear Multiple-Bond Correlation spectroscopy (HMBC), IR, CV, and EPR spectroscopy.

(a) The addition of one equivalent pyridine to the reaction solution of complex **4** and **S5** (1:1 ratio) at room temperature was conducted to understand the possibility of pyridine serving as coordinating ligand to vanadium center of complex **2**. As shown in Figure 3c, the added 1 equiv. pyridine dose not show the characteristic uncoordinated pyridine ^{1}H-NMR signals with chemical shift $\delta > 8$. This result implicates that the coordination of pyridine to the vanadium center of complex **2** and yields the corresponding complex **3**. The observation might indicate that the binding of pyridine and deprotonated **S5** to the vanadium center of complex **2** could be reversible. In the catalytic reaction condition, it is still unclear that whether pyridine or **S5** will bind to vanadium center of complex **2** in the first step.

(b) Upon addition of the **S5**, the proposed oxovanadium-substrate complex **4** is produced: the detailed ^{1}H NMR assignment of **S5** was achieved by a combination of ^{1}H-^{13}C HSQC and ^{1}H-^{1}H COSY spectra (Figure S11). The ^{1}H-NMR of **S5** shows that there are six signals in the range of $\delta = 2.8 - \delta = 5.8$ with total integration area ca. 6 which corresponds to the non-aromatic H signal. The five ^{1}H-NMR peaks were labelled from $\delta = 2.8 - \delta = 5.8$ as H_a ($\delta = 3.76$,1H), H_b (($\delta = 3.48$, 1H), H_c ($\delta = 4.42$, 1H 1H), H_d ($\delta = 2.96$,1H), H_e ($\delta = 4.93$,1H), and H_f ($\delta = 3.68$,1H). The ^{1}H-^{13}C HSQC spectrum shown in Figure S12a allows us to determine the connectivity between H and C atoms which only the directly bonded hydrogen and carbon shows a cross peak. The ^{1}H-^{13}C HSQC spectrum of **S5** indicates that H_a, H_b, H_c, and H_e show cross peaks, suggesting that H_d and H_f are attached to non-carbon atoms. Based on these observations and the chemical structure of **S5**, the H_d and H_f are assigned as the proton signals of alcohol functional group. From the coupling patterns of H_d and H_f shown in the ^{1}H-^{1}H COSY spectrum of **S5** (Figure S12b), H_f only shows one cross-peak between H_f and H_e where H_d has exhibited cross-peaks to both H_a and H_b. Based on the coupling patterns and chemical shifts, the H_f and H_d are assigned as proton signals of benzylic and aliphatic alcohol functional connected to the C_α and $C_{\gamma,}$ respectively. Since H_e shows a cross peak to the benzylic alcohol proton H_f in the COSY spectrum, H_e is then assigned as C_α-H signal. Similarly, H_a and H_b demonstrated two cross peaks associated with aliphatic alcohol proton H_d, which indicates the H_a and H_b are magnetically inequivalent and all bonded to the C_γ. Finally, H_c displays cross peak to H_a, H_b, and H_e, which suggests its connectivity to C_β. Based on the ^{1}H-^{13}C HSQC and ^{1}H-^{1}H COSY spectra of **S5**, the six ^{1}H NMR signals in the range of $\delta = 2.8 - \delta = 5.8$ are

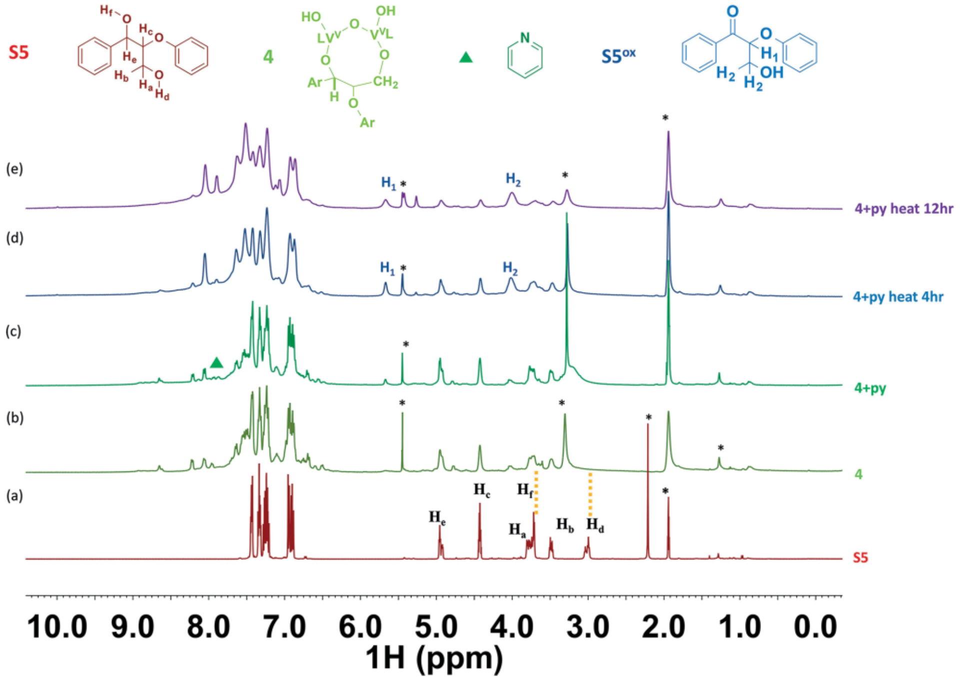

Figure 3. (a) the ^1H NMR of the substrate S5. (b) the ^1H NMR spectrum of the reaction solution of S5 and complex **2** in 1:1 ratio. (c) the ^1H NMR spectrum of the resulting solution c with 1 equivalent pyridine. (d) the ^1H NMR spectrum of the resulting solution d at 80 °C for 4 h (e) the ^1H NMR spectrum of the resulting solution d at 80 °C for 12 h.

assigned. The assignment has been further confirmed by the ^1H-^{13}C HMBC spectrum of **S5** shown in Figure S12c.

The substrate binding mode was probed by the reaction of **S5** and complex **2** in 1:1 ratio under N_2 atmosphere at room temperature to prevent the subsequent catalytical alcohol oxidation. The ^1H-NMR spectrum of reaction solution (Figure 3a–b) reveals the complete disappearance of H_d and H_f peaks, implicating the ability of complex **2** to abstract two alcohol protons of **S5**. The proton abstraction is likely proceeded by two V=O moieties of complex **2** to form a tentative dicationic $[(SBH)(OH)V(\mu\text{-}O)V(OH)(SBH)]^{2+}$ chelated with deprotonated **S5** substrate intermediate **4** (Scheme 4a). The proton abstraction

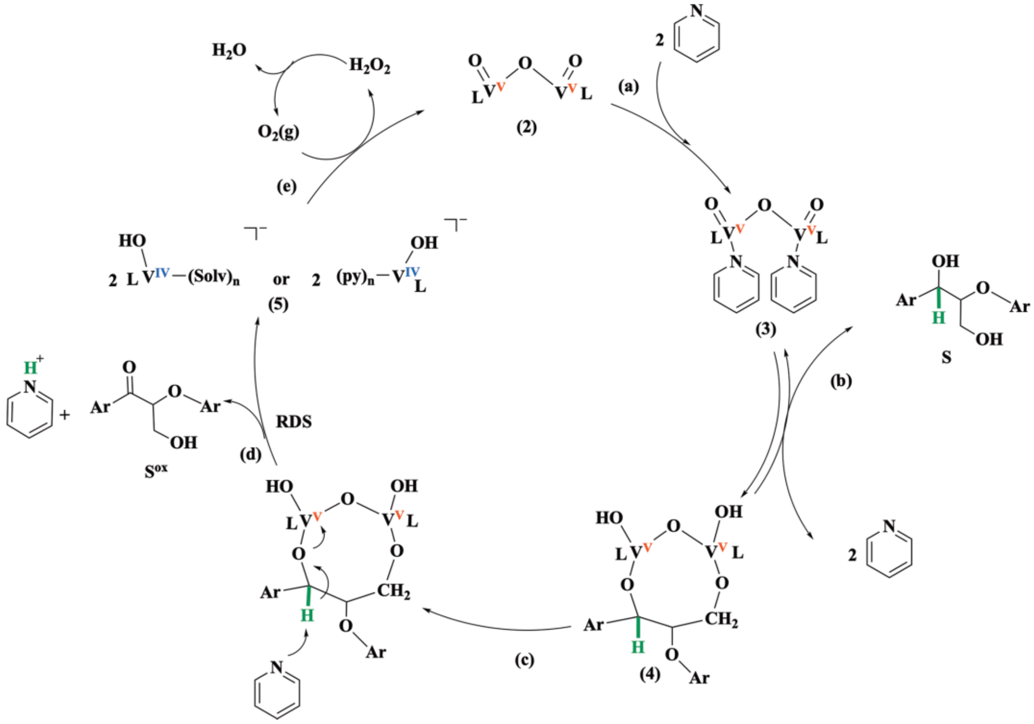

Scheme 4. Proposed catalytic mechanism of selective C_α alcohol oxidation of a lignin substrate containing β-O-4 Linkage.

via two V=O moieties of complex **2** is further supported by the disappearance of characteristic V=O stretching frequency ($\nu_{V=O}$ ca. 964 cm^{-1}) and the growth of O-H stretching frequency (ν_{O-H} ca. 3365 cm^{-1}) (Figure S13).

(c) the role of pyridine on the oxidation of **S5** into **S5^ox^** (rate-determining step): By increasing temperature to 80 °C, the H_e signal of intermediate **4** is decreased (in the presence of 1 equivalent of pyridine) accompanied by the observation characteristic ^1H NMR signal of $\mathbf{S5^{ox}}$ (δ = 3.97, 2H; δ = 5.67 1H) as demonstrated in Figure 3d-e and Scheme 4b. In order to probe the role of pyridine additive, we carried out the catalytic oxidation of lignin model substrate **S5** by using 2,6-lutidine and 4-dimethylaminopyridine as additives, respectively. The selectivity and conversion of these reactions were summarized in Table S2. By using 2,6-lutidine as an additive, there is 0% conversion which clearly indicates the essence of pyridine coordination in order to proceed the catalytic oxidation of lignin substrate **S5**. Interestingly, using 4-dimehylaminopyridine (DMAP) as an additive slightly increase conversion rate (82%) but the selectivity decreases from 97% to 18%. The rationale of this dramatical decrease in selectivity toward benzylic alcohol oxidation is attributed to the formation of unexpected dehydration product $\mathbf{S5^{de}}$ (48% yield). To further investigate the possible pathway of the $\mathbf{S5^{de}}$ formation, we have carried out a reaction using $\mathbf{S5^{ox}}$ and DMPA as substrate and additive, respectively, as well as 5% complex **2** as catalyst. The ^1H-NMR spectrum of this reaction indicates 80% conversion from $\mathbf{S5^{ox}}$ to $\mathbf{S5^{de}}$ (Figure S14). These results suggest that the suitable basicity range of unhindered pyridine derivatives is required for selective oxidation of C_α alcohol without subsequently transforming $\mathbf{S5^{ox}}$ into $\mathbf{S5^{de}}$. To further examine the possibility that DMAP deprotonate $\mathbf{S5^{ox}}$ to yield the corresponding $\mathbf{S5^{de}}$, we mixed $S5^{ox}$ and DMAP in 1:1 ratio at 85 °C for 24 h. As shown in Figure S15, no $\mathbf{S5^{de}}$ formation has been observed.

(d) the spectroscopic characterizations of key mononuclear oxovanadium intermediate **5**: the broad ^1H NMR of the pyridine-deprotonated solution could be attributed to the presence of a paramagnetic specie resulting from the oxidation of C_α alcohol to ketone. To further investigate the nature of the paramagnetic specie, the EPR spectroscopy, Evans method, and cyclic voltammetry experiments had been pursued. The EPR spectrum of the resulting solution (Figure 4a) measured at room temperature had exhibited a well-resolved and characteristic 8-line EPR signal with (g_1 = 1.97, g_2 = 1.98, g_3 = 1.99; $A_{1(V)}$ = 145 G, $A_{2(V)}$ = 110 G, $A_{3(V)}$ = 40 G in the fast motion tumbling regime (correlation time ca. 10^{-10} s) which is the well-documented mononuclear V^{IV} EPR spectrum.[5a,15] The 8-line feature also excludes the possibility of existence of delocalized V^{IV}-V^{V} electronic state which has been shown to display a 15-line EPR signal.[16] In combination with EPR results, the magnetic susceptibility of the paramagnetic species was determined by the Evans method (Figure S15), which corresponds to the formation of two mononuclear V^{IV} intermediates. Based on the above experimental evidence, the paramagnetic species generating by accepting two electrons from the oxidation of S**5** is presumably proposed as two mononuclear oxovanadium intermediate **5** with V^{IV} electronic state (Scheme 4d). The feasibility of intermediate **4** accommodating two electrons to yield the temporarily stable dinuclear V^{IV}-V^{IV} complex before the formation of mononuclear intermediate **5** has been investigated.[17] The solution behavior of the dinuclear V(V) complex containing [V–O-V] structure motif was extensively studied. Based on the investigation, the dinuclear structure of vanadium complex with V(V)-V(V) oxidation state remains intact in solution even with the coordination of pyridine on vanadium center. Upon two electrons reduction, the dinuclear V(IV)-V(IV) complex subsequently transforms into mononuclear V(IV) complex characterized by its distinct 8-line EPR signal. In order to provide more convincing evidence for the possible transformation of dinuclear nature of complex **2** in solution, ^1H-NMR (Figure 3) spectra, CV voltammograms (Figure 4) were conducted. The CV voltammograms of complex **2** and complex **2** coordinated with **S5** both exhibit two reversible redox waves, which also implicates the integrity of dinuclear structure. However, after receiving two electrons from the oxidation of benzyl alcohol, the dinuclear structure of complex **2** may transform into two mononuclear vanadium (IV) species via the coordination of pyridine/solvent as evidenced by its distinct 8-line EPR signal which corresponds to the mononuclear V^{IV} intermediate determined from Evans method. We further examined the possibility by conducting the cyclic voltammetry of intermediate **4**. As shown in Figure 4b, the second

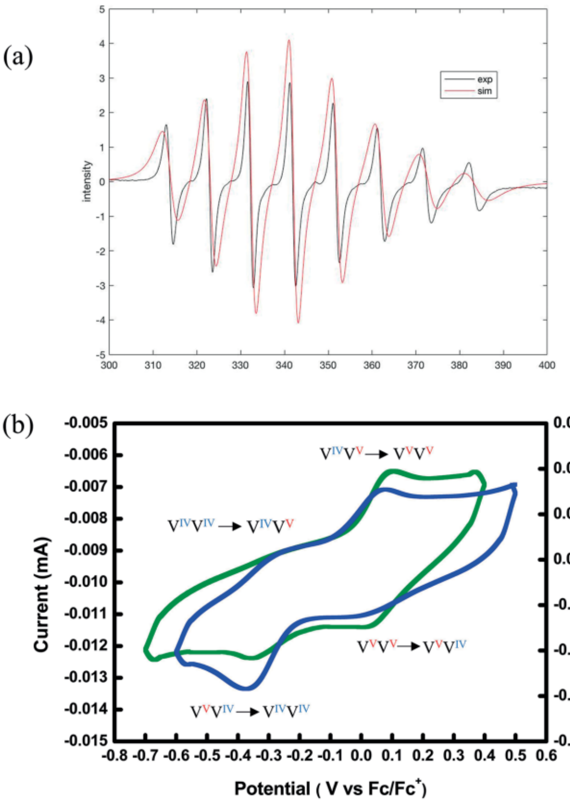

Figure 4. Overlap of the experimental EPR spectrum of reaction solution (**S5** and complex **4** in 1:1 ratio) added with 1 equivalent pyridine at 80 °C for 12 h (black line) and the simulated EPR spectrum with g_1 = 1.97, g_2 = 1.98, g_3 = 1.99; $A_{1(V)}$ = 145 G, $A_{2(V)}$ = 110 G, $A_{3(V)}$ = 40 G; correlation time = $10^{-9.65}$ s^{-1} (red line). (b) the overlapped CV spectra of complex **2** (green line) and intermediate **4** (blue line) measured in CH_3CN solution with a glass carbon working electrode at a scan rate of 50 mV.

Table 4. Current catalyst systems and representative mononuclear vanadium catalysts using O_2 as oxidant for the selective oxidation of benzyl alcohol with a β-O-4 linkage and a C_γ primary alcohol.

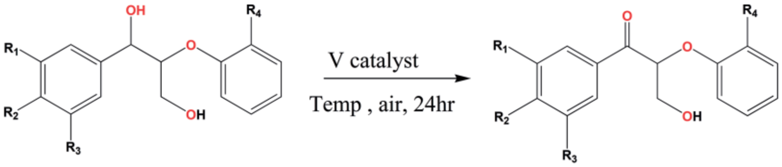

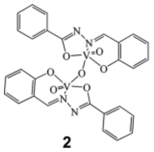
2

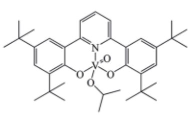
M1

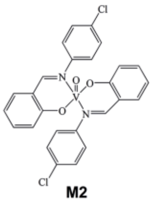
M2

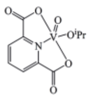
M3

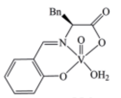
M4

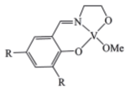
M5

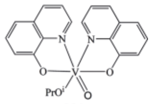
M6

Entry	Substituent	Cat.	Selec. [%][a]	Conv. [%][a]	Yield	T/ °C	Ref.
1	R^1=H, R^2=H, R_3=H, R_4=H	2	97	77	75	80	This work
2	R^1=H, R^2=OMe, R_3=H, R_4=OMe	2	71	55	39	80	This work
3	R^1=H, R^2=OMe, R_3=H, R_4=H	2	89	65	58	80	This work
4	R^1=H, R^2=H, R_3=H, R_4=OMe	2	85	62	53	80	This work
5	R^1=H, R^2=OEt, R_3=OMe, R_4=OMe	V(O)(O*i*Pr)$_3$	55	82	45	80	[7b]
6[b]	R^1=OMe, R^2=H, R_3=OMe, R_4=OMe	V(O)(O*i*Pr)$_3$	52	75	39	100	[7d]
7	R^1=H, R^2=OEt, R_3=OMe, R_4=OMe	V(O)(acac)$_2$	39	79	31	80	[7b]
8[b]	R^1=OMe, R^2=H, R_3=OMe, R_4=OMe	M1	27	84	23	100	[8b]
9[b]	R^1=OMe, R^2=H, R_3=OMe, R_4=OMe	M2	31	85	27	100	[17]
10[b]	R^1=OMe, R^2=H, R_3=OMe, R_4=OMe	M3	68	95	65	100	[7d]
11	R^1=H, R^2=OEt, R_3=OMe, R_4=OMe	M4	68	86	59	80	[7b]
12	R^1=H, R^2=OEt, R_3=OMe, R_4=OMe	M5	62	66	41	80	[7b]
13	R^1=H, R^2=OEt, R_3=OMe, R_4=OMe	M6	28	95	27	80	[7b]
14[b]	R^1=OMe, R^2=H, R_3=OMe, R_4=OMe	M6	85	65	55	80	[7e]

[a] Selec. and Conv. represent selectivity and conversion, respectively. [b] Reaction time = 48 h.

irreversible redox wave observed in the CV spectrum of complex **2** ($E_{1/2}$ ca. –0.335 mV, i_{pc}/i_{pa} ca. 0.1, ΔE_p ca. 111 mV) had presumably changed toward quasi-reversible as indicated in the second redox wave of intermediate **4** ($E_{1/2}$ ca. –0.318 mV, i_{pc}/i_{pa} ca. 0.3, ΔE_p ca. 95 mV). Note that the Fc/Fc^+ redox couple used as an internal standard showed i_{pc}/i_{pa} ca. 0.99 and ΔE_p ca. 75 mV. The different electrochemical behaviors between complex **2** and intermediate **4** implicate that the substrate binding to a dinuclear oxovanadium complex is a key step to facilitate the two-electron transfer receiving from the oxidation of alcohol into ketone.

(e) Regenerating the dinuclear oxovanadium complex **2** from the mononuclear intermediate **5**: the regeneration of dinuclear vanadium complex **2** with V^V-V^V oxidation state was achieved by simply exposing the intermediate **5** with O_2 or air (Scheme 4e). The two-electron transfer from the V^{IV} core of intermediate **5** to O_2 resulted in the formation hydrogen peroxide characterized by H_2O_2 strip qualitatively (Figure S16). The necessity of exposing O_2 to regenerate the complex **2** was verified by conducting the catalytic oxidation reaction under N_2 atmosphere. Only trace amount of **S5^{ox}** was detected as compared to almost 80% conversion under air/O_2 atmosphere. The formation of H_2O, presumably resulting from the decomposition of H_2O_2 at 80 °C, during the catalytic cycle was also observed in the ^1H NMR at ca. δ = 2.6 (Figure S17). To confirm this peak as H_2O, molecular sieves with 4 Å porous size was added. The ^1H NMR signal ca. δ = 2.6 disappeared after incubating the molecular sieves in the resulting solution overnight.

Based on the available experimental and spectroscopic evidence, we have derived the plausible catalytic mechanism associated with selectively oxidizing C_α alcohol of lignin dimeric substrates to ketone via a dinuclear oxovanadium catalysts. The catalytic reaction was presumably initiated by the coordination of pyridine to the vanadium center of complex **2** followed by the deprotonation of the secondary benzylic alcohol and the primary aliphatic alcohol by two V=O motifs to produce the dinuclear vanadium chelated with a deprotonated lignin substrate (Scheme 4a–b). Note that the order of pyridine or a lignin substrate binding to the complex **2** could be arbitrary. Upon coordinating to the dinuclear vanadium core, the acidity of C_α-H of a lignin substrate is likely to increase to facilitate the deprotonation of C_α-H via uncoordinated pyridine (Scheme 4c). In addition, the coordination of the lignin substrate might also provide the facile avenues to accept two electrons yielding the corresponding dinuclear complex with V^{IV}-V^{IV} oxidation state, evidenced by that the intermediate **4** exhibits two redox waves in cyclic voltammetry studies, followed by the formation of the cationic mononuclear intermediate **5** as evidenced from the EPR spectroscopy and Evans method (Scheme 4d). Since the transformation of alcohol into the corresponding ketone is an intrinsic two-electron oxidation process, the highly selective alcohol oxidation (> 85% selectivity) could be attributed to the dinuclear core of oxovanadium complex **2** that is capable of serving as a two-electron reservoir. The oxidations of two proposed mononuclear V^{IV} intermediate **5** via O_2 led to the formation of H_2O_2 which subsequently decomposed into H_2O and O_2 characterized by H_2O_2 strip and ^1H NMR spectrum (Scheme 4e). Note that the overall transformation of C_α alcohol oxidation catalyzed by dinuclear vanadium complex **2** could also be regarded as a net H-atom transfer from the reactive C-H of the benzylic alcohol.

We have summarized the catalytic selectivity and conversion between complex **2** and some representative mononuclear vanadium catalysts in Table 4.[7b,7d,8b,18] In particular, we focus on the alcohol oxidation of non-phenolic lignin model substrates with a β-O-4 linkage mode and primary C_γ alcohol. Since the alcohol oxidations of this research work is using air as oxidant, we compared the results of benzyl alcohol oxidation of lignin model substrates in literature that use air as oxidant. As indicated in the Table 4, the selectivity of C_α alcohol oxidation via the synthesized complex **2** (97% selectivity and 77% conversion**,** entry 1) is enhanced as compared to the listed mononuclear vanadium catalysts (28%-68% selectivity, entries 5–10) with representative vanadium catalysts ($V(O)(O\mathit{i}Pr)_3$, $V(O)(acac)_2$, M1–M6). For the catalyst that performs slightly lower (> 10%) selectivity and conversion (85% selectivity and 65% conversion, entry 11), the reaction time is significantly longer than that in this work (24 hours vs. 48 hours) and using pyridine as solvent. As compared to the listed representative mononuclear vanadium catalysts, we believe that our catalyst system using dinuclear complex **2** as catalyst and pyridine as additive has made significantly scientific advances in the field of selective oxidation of benzyl alcohol in lignin model substrates containing a β-O-4 linkage and a primary C_γ alcohol.

Conclusions

In this study, the catalytic oxidation of C_α alcohol to ketone of lignin dimeric substrates containing β-O-4 linkage has been demonstrated via the catalyst system containing dinuclear oxovanadium complex **2** with one equivalent of pyridine at 80 °C under air. In contrast to the one reversible redox couple of mononuclear oxovanadium catalyst **1** at $E_{1/2} = -0.477$ V, the dinuclear oxovanadium complex **2** exhibits one reversible and one irreversible redox couple at $E_{1/2} = -0.055$ V and $E_{1/2} = -0.335$ V, respectively. Interestingly, the second redox wave of substrate-chelating dinuclear vanadium intermediate **4** displays a quasi-reversible behavior as compared to that of complex **2** (i_{pc}/i_{pa} ca. 0.1, ΔE_p ca. 111 mV for complex **2**; i_{pc}/i_{pa} ca. 0.3, ΔE_p ca. 95 mV for intermediate **4**) implicating that the feasibility of intermediate **4** to exert facile chemical transformations involving two-electron redox shuffling. Since the oxidation of alcohol to ketone is a classical two-electron oxidation reaction, the highly selective oxidation of C_α alcohol to ketone of various lignin dimeric substrates may be rationalized by the two-electron capacity of dinuclear vanadium core, in contrast to the reported one-electron pathway involving ketyl radical intermediate and a subsequent C-O bond cleavage.

The catalytic mechanism has been proposed and divided into several elementary steps involving (1) the coordination of pyridine to the vanadium center of complex **2** and deprotonation of secondary benzylic alcohol as well as primary aliphatic alcohol located at the C_α and C_γ by the two V=O motifs of dinuclear oxovanadium complex **2**, respectively, characterized by the ^1H NMR and IR spectra. Therefore, the preservation of V=O motif could be crucial for the binding of lignin substrates to vanadium catalysts. (2) abstracting the C_α-H of deprotonated lignin substrates chelating on dinuclear vanadium core via pyridine followed by a two-electron transfer to the dinuclear vanadium core of intermediate **4** to form a transient stable dinuclear vanadium with a V^{IV}-V^{IV} oxidation state and subsequently cleave into two mononuclear intermediate **5** with V^{IV} oxidation state which has been characterized by its distinct 8-line feature of V^{IV} EPR spectrum and a magnetic susceptibility determined by Evans method.[17] (3) regenerating the dinuclear oxovanadium complex **2** by reacting the two mononuclear V^{IV} intermediate **5** with O_2 or air and producing H_2O_2 by-product, which decomposes into H_2O and O_2 at 80 °C, evidenced by a H_2O_2 test strip and ^1H NMR spectra, respectively.

The excellent selectivity of dinuclear oxovanadium complex **2** could be attributed to the intrinsic nature of dinuclear vanadium core that is capable of serving as a two-electron reservoir in order to facilitate the oxidation of alcohol into ketone (also a well-known two-electron oxidation reaction). The mechanistic insights regarding the relationships between the molecular/electronic structure of the dinuclear oxovanadium catalyst and the chemical reactivity of selective oxidation of C_α alcohol to ketone of lignin dimeric substrates featuring a β-O-4 linkage mode could be beneficial to the rational design of highly efficient and selective molecular catalysts for harnessing lignin biomass via two-step strategy.

Experimental Section

The detailed experimental procedures of synthesis of lignin dimeric substrates, oxovanadium complexes, measurement of cyclic voltammogram, EPR were included in the supporting information. The ^1H, ^{13}C, ^{51}V NMR spectra of complex **1** and **2**; the HMBC spectrum of S5; the overlapped IR spectrum of complex **2** and intermediate **4**; the ^1H NMR spectrum of Evans method; the picture of H_2O_2 test strip.

CCDC 1884038 (for 2) contains the supplementary crystallographic data for this paper. These data can be obtained free of charge from The Cambridge Crystallographic Data Centre.

Acknowledgments

We gratefully acknowledge financial support from the Ministry of Science and Technology (Taiwan). We also thank the National

Center for High-Performance Computing (NCHC) for their support on the hardware and software applied in this work. The authors thank Mr. Ting-Shen Kuo for single-crystal X-ray structural determinations.

Keywords: Biomass · Lignin · Vanadium · Homogeneous catalysis · Redox chemistry

[1] a) Z. Sun, B. Fridrich, A. de Santi, S. Elangovan, K. Barta, *Chem. Rev.* **2018**, *118*, 614–678; b) Z. Sun, G. Bottari, A. Afanasenko, M. C. A. Stuart, P. J. Deuss, B. Fridrich, K. Barta, *Nat. Catal.* **2018**, *1*, 82–92; c) W. Leitner, J. Klankermayer, S. Pischinger, H. Pitsch, K. Kohse-Höinghaus, *Angew. Chem. Int. Ed.* **2017**, *56*, 5412–5452; *Angew. Chem.* **2017**, *129*, 5500; d) R. Rinaldi, R. Jastrzebski, M. T. Clough, J. Ralph, M. Kennema, P. C. A. Bruijnincx, B. M. Weckhuysen, *Angew. Chem. Int. Ed.* **2016**, *55*, 8164–8215; *Angew. Chem.* **2016**, *128*, 8296; e) M. Wang, J. Ma, H. Liu, N. Luo, Z. Zhao, F. Wang, *ACS Catal.* **2018**, *8*, 2129–2165; f) W. Schutyser, T. Renders, S. Van den Bosch, S. F. Koelewijn, G. T. Beckham, B. F. Sels, *Chem. Soc. Rev.* **2018**, *47*, 852–908.

[2] M. D. Kärkäs, B. S. Matsuura, T. M. Monos, G. Magallanes, C. R. J. Stephenson, *Org. Biomol. Chem.* **2016**, *14*, 1853–1914.

[3] a) P. J. Deuss, K. Barta, *Coord. Chem. Rev.* **2016**, *306*, 510–532; b) C. Li, X. Zhao, A. Wang, G. W. Huber, T. Zhang, *Chem. Rev.* **2015**, *115*, 11559–11624; c) M. Wang, L. H. Li, J. M. Lu, H. J. Li, X. C. Zhang, H. F. Liu, N. C. Luo, F. Wang, *Green Chem.* **2017**, *19*, 702–706; d) M. Dawange, M. V. Galkin, J. S. M. Samec, *ChemCatChem* **2015**, *7*, 401–404.

[4] a) P. C. Bruijnincx, B. M. Weckhuysen, *Nat. Chem.* **2014**, *6*, 1035–1036; b) J. Zakzeski, P. C. A. Bruijnincx, A. L. Jongerius, B. M. Weckhuysen, *Chem. Rev.* **2010**, *110*, 3552–3599.

[5] a) M. Mahroof-Tahir, A. D. Keramidas, R. B. Goldfarb, O. P. Anderson, M. M. Miller, D. C. Crans, *Inorg. Chem.* **1997**, *36*, 1657–1668; b) J. M. Nichols, L. M. Bishop, R. G. Bergman, J. A. Ellman, *J. Am. Chem. Soc.* **2010**, *132*, 12554–12555; c) A. G. Sergeev, J. F. Hartwig, *Science* **2011**, *332*, 439–443; d) J. Zakzeski, A. L. Jongerius, P. C. A. Bruijnincx, B. M. Weckhuysen, *ChemSusChem* **2012**, *5*, 1602–1609; e) J. He, C. Zhao, J. A. Lercher, *J. Am. Chem. Soc.* **2012**, *134*, 20768–20775; f) T. vom Stein, T. den Hartog, J. Buendia, S. Stoychev, J. Mottweiler, C. Bolm, J. Klankermayer, W. Leitner, *Angew. Chem. Int. Ed.* **2015**, *54*, 5859–5863; *Angew. Chem.* **2015**, *127*, 5957; g) J.-w. Zhang, G.-p. Lu, C. Cai, *Green Chem.* **2017**, *19*, 4538–4543.

[6] a) S. Jia, B. J. Cox, X. Guo, Z. C. Zhang, J. G. Ekerdt, *ChemSusChem* **2010**, *3*, 1078–1084; b) V. M. Roberts, V. Stein, T. Reiner, A. Lemonidou, X. Li, J. A. Lercher, *Chem. Eur. J.* **2011**, *17*, 5939–5948; c) T. Kleine, J. Buendia, C. Bolm, *Green Chem.* **2013**, *15*, 160–166; d) M. R. Sturgeon, S. Kim, K. Lawrence, R. S. Paton, S. C. Chmely, M. Nimlos, T. D. Foust, G. T. Beckham, *ACS Sustainable Chem. Eng.* **2014**, *2*, 472–485; e) S. Dabral, J. Mottweiler, T. Rinesch, C. Bolm, *Green Chem.* **2015**, *17*, 4908–4912; f) C. W. Lahive, P. J. Deuss, C. S. Lancefield, Z. Sun, D. B. Cordes, C. M. Young, F. Tran, A. M. Z. Slawin, J. G. de Vries, P. C. J. Kamer, N. J. Westwood, K. Barta, *J. Am. Chem. Soc.* **2016**, *138*, 8900–8911; g) A. Rodriguez, D. Salvachúa, R. Katahira, B. A. Black, N. S. Cleveland, M. Reed, H. Smith, E. E. K. Baidoo, J. D. Keasling, B. A. Simmons, G. T. Beckham, J. M. Gladden, *ACS Sustainable Chem. Eng.* **2017**, *5*, 8171–8180.

[7] a) S. K. Hanson, R. T. Baker, J. C. Gordon, B. L. Scott, D. L. Thorn, *Inorg. Chem.* **2010**, *49*, 5611–5618; b) S. Son, F. D. Toste, *Angew. Chem. Int. Ed.* **2010**, *49*, 3791–3794; *Angew. Chem.* **2010**, *122*, 3879; c) J. Zakzeski, P. C. A. Bruijnincx, B. M. Weckhuysen, *Green Chem.* **2011**, *13*, 671–680; d) B. Sedai, C. Díaz-Urrutia, R. T. Baker, R. Wu, L. A. P. Silks, S. K. Hanson, *ACS Catal.* **2011**, *1*, 794–804; e) S. K. Hanson, R. Wu, L. A. P. Silks, *Angew. Chem. Int. Ed.* **2012**, *51*, 3410–3413; *Angew. Chem.* **2012**, *124*, 3466; f) A. Wu, B. O. Patrick, E. Chung, B. R. James, *Dalton Trans.* **2012**, *41*, 11093–11106; g) T. Rinesch, J. Mottweiler, M. Puche, P. Concepción, A. Corma, C. Bolm, *ACS Sustainable Chem. Eng.* **2017**, *5*, 9818–9825; h) S. Dabral, J. G. Hernández, P. C. J. Kamer, C. Bolm, *ChemSusChem* **2017**, *10*, 2707–2713; i) Y. Ma, Z. Du, J. Liu, F. Xia, J. Xu, *Green Chem.* **2015**, *17*, 4968–4973; j) W. Schutyser, S. Van den Bosch, J. Dijkmans, S. Turner, M. Meledina, G. Van Tendeloo, D. P. Debecker, B. F. Sels, *ChemSusChem* **2015**, *8*, 1805–1818; k) B. Sedai, R. T. Baker, *Adv. Synth. Catal.* **2014**, *356*, 3563–3574; l) A. Barbieri, J. B. Kasper, F. Mecozzi, O. Lanzalunga, W. R, Browne, *ChemSusChem* **2019**, *12*, 3126–3133; m) R. Gao, Y. Li, H. Kim, J. K. Mobley, J. Ralph, *ChemSusChem* **2018**, *11*, 2045–2050.

[8] a) S. K. Hanson, R. T. Baker, *Acc. Chem. Res.* **2015**, *48*, 2037–2048; b) G. Zhang, B. L. Scott, R. Wu, L. A. P. Silks, S. K. Hanson, *Inorg. Chem.* **2012**, *51*, 7354–7361; c) Y.-Y. Jiang, L. Yan, H.-Z. Yu, Q. Zhang, Y. Fu, *ACS Catal.* **2016**, *6*, 4399–4410.

[9] J. M. W. Chan, S. Bauer, H. Sorek, S. Sreekumar, K. Wang, F. D. Toste, *ACS Catal.* **2013**, *3*, 1369–1377.

[10] a) S. Gazi, W. K. Hung Ng, R. Ganguly, A. M. Putra Moeljadi, H. Hirao, H. S. Soo, *Chem. Sci.* **2015**, *6*, 7130–7142; b) S. Gazi, M. Đokić, A. M. P. Moeljadi, R. Ganguly, H. Hirao, H. S. Soo, *ACS Catal.* **2017**, *7*, 4682–4691; c) N. Luo, M. Wang, H. Li, J. Zhang, H. Liu, F. Wang, *ACS Catal.* **2016**, *6*, 7716–7721; d) M. D. Karkas, I. Bosque, B. S. Matsuura, C. R. Stephenson, *Org. Lett.* **2016**, *18*, 5166–5169; e) J. D. Nguyen, B. S. Matsuura, C. R. Stephenson, *J. Am. Chem. Soc.* **2014**, *136*, 1218–1221; f) J. Dai, A. F. Patti, G. N. Styles, S. Nanayakkara, L. Spiccia, F. Arena, C. Italiano, K. Saito, *Green Chem.* **2019**, *21*, 2005–2014.

[11] A. Rahimi, A. Ulbrich, J. J. Coon, S. S. Stahl, *Nature* **2014**, *515*, 249–252.

[12] a) M. Wang, J. Lu, X. Zhang, L. Li, H. Li, N. Luo, F. Wang, *ACS Catal.* **2016**, *6*, 6086–6090; b) T. Hou, N. Luo, H. Li, M. Heggen, J. Lu, Y. Wang, F. Wang, *ACS Catal.* **2017**, *7*, 3850–3859; c) A. Rahimi, A. Azarpira, H. Kim, J. Ralph, S. S. Stahl, *J. Am. Chem. Soc.* **2013**, *135*, 6415–6418; d) K. Walsh, H. F. Sneddon, C. J. Moody, *Org. Lett.* **2014**, *16*, 5224–5227; e) C. S. Lancefield, O. S. Ojo, F. Tran, N. J. Westwood, *Angew. Chem. Int. Ed.* **2015**, *54*, 258–262; *Angew. Chem.* **2015**, *127*, 260–264; f) R. Zhu, B. Wang, M. Cui, J. Deng, X. Li, Y. Ma, Y. Fu, *Green Chem.* **2016**, *18*, 2029–2036; g) S. Dabral, H. Wotruba, J. G. Hernández, C. Bolm, *ACS Sustainable Chem. Eng.* **2018**, *6*, 3242–3254.

[13] J. Luo, X. Zhang, J. Lu, J. Zhang, *ACS Catal.* **2017**, *7*, 5062–5070.

[14] a) E. Ludwig, U. Schilde, E. Uhlemann, F. Weller, K. Dehnicke, *Z. Anorg. Allg. Chem.* **1993**, *619*, 669–674; b) A. Sundheim, R. Mattes, *Z. Naturforsch. B* **1993**, *48*, 1848–1850; c) N. R. Sangeetha, S. Pal, *Bull. Chem. Soc. Jpn.* **2000**, *73*, 357–363.

[15] a) V. A. Tuskaev, N. A. Kolosov, D. A. Kurmaev, S. C. Gagieva, V. N. Khrustalev, N. S. Ikonnikov, N. N. Efimov, E. A. Ugolkova, V. V. Minin, B. M. Bulychev, *J. Organomet. Chem.* **2015**, *798*, 393–400; b) M. Thirumavalavan, A. M. Martins, *Inorg. Chem. Commun.* **2006**, *9*, 497–499; c) S. Aharonovich, M. Botoshansky, B. Tumanskii, K. Nomura, R. M. Waymouth, M. S. Eisen, *Dalton Trans.* **2010**, 39.

[16] a) S. K. Dutta, S. B. Kumar, S. Bhattacharyya, E. R. T. Tiekink, M. Chaudhury, *Inorg. Chem.* **1997**, *36*, 4954–4960; b) A. Mondal, S. Sarkar, D. Chopra, T. N. Guru Row, K. Pramanik, K. K. Rajak, *Inorg. Chem.* **2005**, *44*, 703–708; c) S. P. Dash, S. Roy, M. Mohanty, M. F. Carvalho, M. L. Kuznetsov, J. C. Pessoa, A. Kumar, Y. P. Patil, A. Crochet, R. Dinda, *Inorg. Chem.* **2016**, *55*, 8407–8421.

[17] S. P. Dash, S. Majumder, A. Banerjee, M. F. N. N. Carvalho, P. Adão, J. C. Pessoa, K. Brzezinski, E. Garribba, H. Reuter, R. Dinda, *Inorg. Chem.* **2016**, *55*, 1165–1182.

[18] a) C. Díaz-Urrutia, B. Sedai, K. C. Leckett, R. T. Baker, S. K. Hanson, *ACS Sustainable Chem. Eng.* **2016**, *4*, 6244–6251; b) S. K. Hanson, R. T. Baker, J. C. Gordon, B. L. Scott, L. A. P. Silks, D. L. Thorn, *J. Am. Chem. Soc.* **2010**, *132*, 17804–17816; c) S. K. Hanson, R. Wu, L. A. P. Silks, *Org. Lett.* **2011**, *13*, 1908–1911.

Received: July 24, 2019